The Use of Side Wall Images to Compute Package Effects in MoM Analysis of MMIC Circuits

Robert W. Jackson, *Senior Member, IEEE*

Abstract— **A novel formulation is presented for the method of moments solution of shielded, enclosed microstrip MMIC circuits. The technique involves first computing a circuit's mutual impedance characteristics with no lateral enclosure and then adding a correcting term resulting from the images introduced by lateral side walls. The method is especially useful for determining the impact of low Q package resonances in very large packages. Large lateral enclosure size does not degrade the efficiency of this technique. The importance of the TM_0 parallel plate mode in MMIC circuit coupling is emphasized.**

I. Introduction

FULL WAVE analysis of planar microstrip circuits has been used for over a decade now [1]–[9] and recent progress has been such that several commercial products are available for fully electromagnetic modeling of relatively simple microstrip structures. The MMIC designer who uses such simulators normally performs an electromagnetic analysis on a small circuit component, a T junction for example, and determines it N-port circuit parameters. These are then entered into a standard circuit analysis package which can analyze the behavior of the over-all MMIC circuit, an amplifier for example. Most electromagnetic simulators surround their analysis space with a perfectly conducting theoretical box [7], [10]–[14]. For reasons of numerical efficiency, this analysis enclosure is normally much smaller than the enclosure that will house the final circuit or circuits. This can make the results of the electromagnetic analysis difficult to interpret, as resonances and proximity effects which occur in one enclosure may be different in the other. The influence of the enclosure and an analysis technique which can include or remove the enclosure's effect are the subjects of this paper.

The future trend toward higher frequencies and higher integration levels is likely to make the aforementioned partitioning process of MMIC design more difficult to implement. Designers are likely to increase the size of the portion of an MMIC to be simulated so as to include coupling from as many different sources as possible. This will require the use of an electrically large analysis enclosure which will be subject to enclosure resonances. Such resonances have a very significant effect on circuit simulations [14], [15]. It will therefore be difficult to have any faith that the simulated N-Port parameters of the circuit portion will accurately predict he behavior in an operating package with a different set of resonances. Clearly, such difficulties must be minimized by insuring that both the analysis enclosure and the operating enclosure be low Q and have only highly damped resonances [16]. Lowering the Q dramatically reduces resonance influence, but even highly damped resonances can have subtle effects and it is difficult to know when these effects are sufficiently eliminated. In some cases the effect of high Q resonances in the physical package can be modeled using circuit models developed by Jansen [17], [18] and by Burke [19]. Both models become complicated for a large detailed structures and when a number of resonances occur in a bandwidth. Thus they will have limited applicability to the low Q, many resonance enclosure which is likely to be of interest in the future.

In this paper, we present a new method of applying the spectral domain moment method to enclosed microstrip circuits. The mutual coupling between current elements on a circuit are first calculated as though the circuit were not laterally enclosed. A correction is then added representing the effect of the image currents which are introduced by the lateral enclosure. The first calculation involves a relatively lengthy spectral integration which results in impedances that are slowly varying with respect to frequency and thus can be interpolated using only a few evaluations in a band. The second calculation, the correction term, must be evaluated at many frequencies in a band depending on the number of enclosure resonances and their Q. It is however very easy to calculate. The total method of moments matrix is formed by summing the two calculations. The numerical advantages to this method are similar to the advantages of the Spectral Operator Expansion [20]. However, the method we describe here is completely different. It has the advantage of being able to add or remove the correction term in order to see the sidewall effects. It is also very intuitive. Its simplicity is based on the dominant effect that the TM_o parallel plate mode has on enclosure coupling. It remains efficient for enclosures with high or low Q having any lateral size, but it is limited to structures with a top cover.

In all of what follows, a configuration similar to Fig. 1 is being discussed. The structure consists of a perfectly conducting ground plane, a dielectric layer supporting the microstrip circuit, a free space layer, a lossy cover substrate, and a perfectly conducting top cover. The purpose of the lossy cover is to lower the enclosure Q. A doped silicon cover substrate is assumed since it is inexpensive, plentiful, and well characterized.

In Section II, the mutual impedance between laterally unenclosed, not too closely spaced currents is written analytically

Manuscript received January 21, 1992; revised July 28, 1992.

The author is with the Department of Electrical and Computer Engineering, University of Massachusetts, Amherst, MA 01003.

IEEE Log Number 9205450.

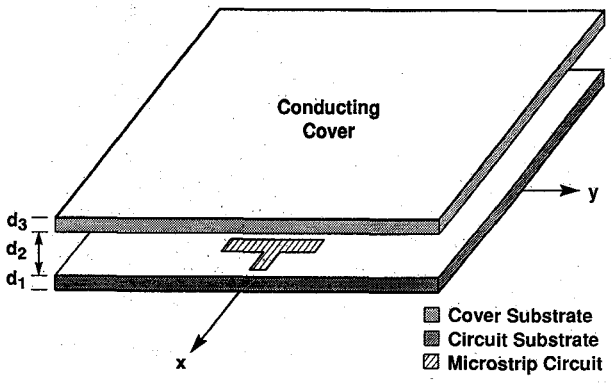

Fig. 1. Layered structure in the interior of an MMIC enclosure. Cover substrate acts to damp enclosure resonances.

based on the TM_o parallel plate wave. In Section III, we describe the use of images to determine the enclosure correction. Modifications to the analysis for circuit pieces located close to or on a sidewall are discussed in Section IV. A concluding discussion is presented in Section V.

II. Mutual Impedance Based on a Parallel Plate Wave

A fundamental part of the moment method analysis of microstrip circuits involves computation of the mutual impedance between two surface currents. A representative mutual impedance between two x directed currents is for example,

$$Z_{ij}^{xx} = -\int\int dx\,dy\,J_{xi}(x,y)[E_x(x,y)]_j \tag{1a}$$

$$= -\int\int dx\,dy\,J_{xi}(x,y) \cdot \int\int dx'\,dy'\,G_{xx}(x,x',y,y')\,J_{xj}(x',y') \tag{1b}$$

with the Green's function, G_{xx}, can be written in terms of TM_z and TE_z parts according to,

$$G_{xx}(x,x',y,y') = \frac{\partial^2}{\partial x^2}G^{\mathrm{TM}}(x,x',y,y') + \frac{\partial^2}{\partial y^2}G^{\mathrm{TE}}(x,x',y,y') \tag{2a}$$

$$G_{xy}(x,x',y,y') = \frac{\partial}{\partial x}\frac{\partial}{\partial y} \cdot [G^{\mathrm{TM}}(x,x',y,y') - G^{\mathrm{TE}}(x,x',y,y')] \tag{2b}$$

G_{xy} is included for completeness. G_{yy} and G_{xy} can be obtained by interchanging the x and y derivatives. For an open structure the TM or TE Green's functions, G^{TM} and G^{TE}, can be expressed in spectral form as

$$G^{\mathrm{TV}}(x,x',y,y') = \frac{1}{2\pi} \cdot \int\int dk_x\,dk_y \frac{Q_{\mathrm{TV}}(\beta)}{\beta^2} e^{jk_x(x-x')}e^{jk_y(y-y')} \tag{3}$$

where V is M or $E, \beta^2 = k_x^2 + k_y^2. Q_{\mathrm{TV}}(\beta)$ is listed in Appendix I and is derived along the lines of reference [21]. The impedance described by (1) includes all sources of coupling between the ith ad jth currents. For an open structure, these sources may include reactive fields, radiation, and surface waves. In the covered structures discussed in this paper the only sources of coupling are reactive fields and the TM_o parallel plate wave. Although expression (3) is written as though no sidewalls are present (k_x, k_y continuous), in the next section it will also be used to derive the effects of side walls.

In many cases of interest it is desirable to have the mutual impedance between two current elements that are not very closely spaced. It then becomes convenient to rewrite (3) in terms of sums of TM and TE parallel plate waves as derived in what follows. Changing the integral in (3) to polar form yields

$$G^{\mathrm{TV}}(\rho) = \frac{1}{2\pi}\int_o^\infty d\beta \frac{Q_{\mathrm{TV}}(\beta)}{\beta} J_o(\beta\rho) = \frac{1}{2\pi}\int_{-\infty}^\infty d\beta \frac{Q_{\mathrm{TV}}(\beta)}{2\beta} H_o^{(2)}(\beta\rho) \tag{4}$$

where $\rho^2 = |x-x'|^2 + |y-y'|^2$. Q_{TM} and Q_{TE} have sets of poles which correspond to the TM and TE parallel plate mode propagation constants.

Such poles are determined from

$$Y_M(\beta_n^{\mathrm{TM}}) = 0; \qquad n = 0,1,2,3\cdots \tag{5a}$$

$$Y_E(\beta_n^{\mathrm{TE}}) = 0; \qquad n = 1,2,3\cdots \tag{5b}$$

$$\mathrm{Re}(\beta_n^{\mathrm{TV}}) > 0; \qquad \mathrm{Im}(\beta_n^{\mathrm{TV}}) < 0$$

where Y_M and Y_E are defined in Appendix I. By closing a contour integration around the lower half of the complex β plane, (4) becomes

$$G^{\mathrm{TV}}(\rho) = -j\sum_n \mathrm{Res}[Q_{\mathrm{TV}}(\beta_n^{\mathrm{TV}})]H_o^{(2)}(\beta_o^{\mathrm{TV}}\rho)/2\beta_n^{\mathrm{TV}} \tag{6}$$

where $\mathrm{Res}[Q(\beta_n)]$ denotes the residue of Q at β_n. Thus the x directed electric field due to an x directed surface current at $z = d$ is, according to (2a),

$$E_x(x,y) = \frac{\partial^2}{\partial x^2}\sum_{n=0}^\infty \frac{-j}{2\beta_n^{\mathrm{TM}}} \cdot \mathrm{Res}[Q_{\mathrm{TM}}(\beta_n^{\mathrm{TM}})]R_n^{x\mathrm{TM}}(x,y) + \frac{\partial^2}{\partial y^2}\sum_{n=1}^\infty \frac{-j}{2\beta_n^{\mathrm{TE}}} \cdot \mathrm{Res}[Q_{\mathrm{TE}}(\beta_n^{\mathrm{TE}})]R_n^{x\mathrm{TE}}(x,y) \tag{7a}$$

where

$$R_n^{x\mathrm{TV}} \equiv \iint_{-\infty}^{\infty} dx'\,dy'\,J_x(x',y')tH_o^{(2)}(\beta_n^{\mathrm{TV}}|\vec{\rho}-\vec{\rho}'|) \tag{7b}$$

and $|\vec{\rho}-\vec{\rho}'| \equiv ([x-x']^2 + [y-y']^2)^{1/2}$ with the $\vec{\rho}, \vec{\rho}'$ dependence explicitly noted.

In the MMIC environment with layering such as is shown in Fig. 1, usually only the lowest order parallel plate mode, the TM_o mode, is propagating while all the other modes are

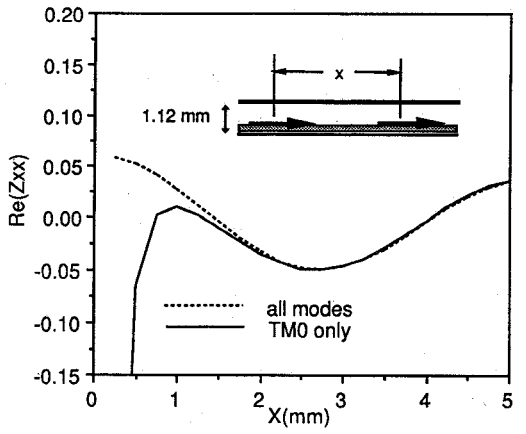

Fig. 2. Mutual impedance calculated using the TM_0 mode only compared to mutual impedance calculated using the full spectrum. The substrate is 0.125 mm GaAs and the operating frequency is 60 GHz. The current elements are rooftop functions 0.125 mm wide and 0.250 mm long.

evanescent. Since $H_o(\beta_n^{\mathrm{TV}}\rho) \propto \exp(-j\beta_n^{\mathrm{TV}}\rho)/\sqrt{\rho}$ for large ρ and since all β_n^{TV} except β_o^{TM} are primarily imaginary, all $R_n^{x\mathrm{TM}}$ and $R_n^{x\mathrm{TE}}$ decay to zero for large ρ except for $R_o^{x\mathrm{TM}}$. Thus, for relatively large ρ, only the TM_o term in (7) is important and

$$E_x(x,y) \approx \frac{-j}{2\beta_o^{\mathrm{TM}}}\mathrm{Res}[Q_{\mathrm{TM}}(\beta_o^{\mathrm{TM}})]\frac{\partial^2}{\partial x^2}R_o^{x\mathrm{TM}}(x,y). \quad (8)$$

For smaller ρ the reactive fields of the evanescent modes are important and more terms in (7) must be included.

Expression (8) can be used to evaluate (1) in cases where the ith and jth currents are well separated. [15], [22]. It is generally the case that the subsectional basis functions (and even groups of basis functions) used in moment method solutions are small enough that $\Delta x\beta_o^{\mathrm{TM}} \ll 1$ where Δx is the scale length of the basis function. As a result (1) can be written:

$$Z_{ij}^{xx} \approx \frac{-j}{2\beta_o^{\mathrm{TM}}}\mathrm{Res}[Q_{\mathrm{TM}}(\beta_o^{\mathrm{TM}})] \cdot \frac{\partial^2}{\partial x_i^2}H_o^{(2)}(\beta_o^{\mathrm{TM}}|\vec{\rho}_i - \vec{\rho}_j|)\langle J_{xi}\rangle\langle J_{xj}\rangle \quad (9)$$

where $\langle J_{xi}\rangle = \int\int dx\,dy\,J_{xi}(x,y)$ and $\vec{\rho}_k$ locates the center of the kth current.

Fig. 2 shows mutual impedance versus separation for two rooftop currents in a representative MMIC environment. The approximation expression (9) is compared to the exact calculation computed from the full spectral integration in (3). In addition to (9) we have also approximated $H_o^{(2)}(x) \approx (2j/x\pi)^{1/2}\exp(-jx)$. For separations greater than 2 mm the curves are identical. We conclude that (1) the coupling between even not very distant currents is principally due to the TM_o parallel plate wave and (2) this coupling does not depend upon the fine details of the currents, only on average quantities so long as the currents are much smaller in extent than a parallel plate wavelength. We will make use of this simplified expression in the next sections.

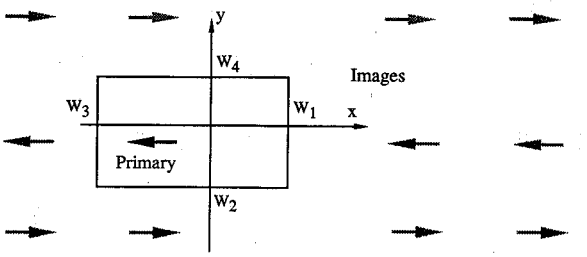

Fig. 3. Schematic drawing of an enclosed current and a few of the infinite set of image currents.

III. Package Effects in Terms of Side Wall Images

In what follows, we show that the method of moments mutual impedance between two currents in an enclosure can be calculated by first calculating the mutual impedance in a laterally open structure and then adding a modifying term which includes the effect of the enclosure side walls. The modifying term is easily computed and makes use of the approximation described in the last section.

Fig. 3 shows a top view of Fig. 1 with a primary source current and the infinite set of images introduced when perfectly conducting side walls are located at $x = W_1$ and W_3 and at $y = W_2$ and W_4. The electric field at a point can be divided into two parts:

$$E_x(x,y) = E_x^{\mathrm{pri}}(x,y) + E_x^{\mathrm{img}}(x,y)$$

The first part is the field resulting from the primary source current in a laterally open structure and the other results from the infinite set of image sources which occur due to the presence of side walls. The field point is often close to or on the primary source current, thus an accurate computation of E_x^{pri} will require all the reactive terms in (6) (or (4)). In most cases however, the image sources are far enough from the field point that only the TM_o mode radiating from each image has any significant contribution to E_x^{img}. This field component is thus simpler to compute. The simplicity is helpful since the image contribution carries much of the frequency dependence of E_x and often must be computed at many points in the bandwidth of interest. An efficient way of combining the effect of the infinite set of image sources will now be discussed.

The total current, consisting of the primary and image currents, can be written as

$$J_x(x,y) = f^t(x)\,g^t(y) \quad (11a)$$

$$f^t(x) = \sum_{n=-\infty}^{\infty}[f(x-2na) + f(2W_1 - x + 2na)] \quad (11b)$$

$$g^t(y) = \sum_{m=-\infty}^{\infty}[g(y-2mb) - g(2W_4 - y + 2mb)] \quad (11c)$$

where the functional dependence of a primary current is just $f(x)\,g(y)$, $a = W_1 - W_3$, and $b = W_4 - W_2$. The field at a point within the package, in principle, can be evaluated by inserting (11) into (7b) and then (7a).

The image currents alone can be written as

$$J_x^{\text{img}} = f^t(x)\, g^t(y) - f(x)\, g(y) \tag{12}$$

Assume the jth primary current is specified by $f_j(x)\, g_j(y)$ and is non-zero only in a vicinity centered around the point (x_j, y_j) located inside the enclosure. The images of this current are all located outside the package, in most cases relatively far from the interior field point (x, y). Thus, for evaluating the contribution of image currents to the interior E field, only the $n = 0$ term of (7a) is important. Furthermore, if the images of the jth primary current are located at (x_α, y_β), then the image portion of $R_o^{x\text{TM}}$ can be written

$$\begin{aligned}(R_{oj}^{x\text{TM}})^{\text{img}} &= \iint_{-\infty}^{\infty} dx'\, dy' \\ &\quad \cdot \sum_{\alpha,\beta} s_\beta f_j(x' - x_\alpha + x_j)\, g_j(y' - y_\beta + y_j) \\ &\quad \cdot H_0^{(2)}(\beta_0^{\text{TM}} \sqrt{(x-x')^2 + (y-y')^2}) \qquad (13a) \\ &\approx \langle J_{xj}\rangle \sum_{\alpha,\beta} s_\beta H_0^{(2)}(\beta_o^{\text{TM}} \sqrt{(x-x_\alpha)^2 + (y-y_\beta)^2}) \qquad (13b)\end{aligned}$$

where the polarity of the image contribution is controlled by $s_\beta = \pm 1$ which in turn depends upon y_β for the x directed current under consideration. If f_j and g_j are non-zero in a small range $\Delta\rho$ around (x_j, y_j) such that $\Delta\rho\beta_o^{\text{TM}} \ll 1$, then (x', y') in the Hankel function argument of (13a) can be approximated by (x_α, y_β) and (13b) results. We define $\langle J_{xj}\rangle$ as in equation (9). Note that the effect of the images only depends upon the average value of the current element.

If the double sum in (13b) were to be evaluated numerically by directly summing over α and β, an enormous number of terms need to be taken before the result converges. In Appendix II it is shown that (13b) can be rewritten in a form which can be very efficiently evaluated.

From (8) and (13b) the interior field resulting from all the images of the jth current is,

$$[E_x^{\text{img}}(x,y)]_j = \frac{-j}{2\beta_o^{\text{TM}}} \text{Res}[Q_{\text{TM}}(\beta_o^{\text{TM}})] \frac{\partial^2}{\partial x^2} \{R_{oj}^{x\text{TM}}\}^{\text{img}} \tag{14}$$

where it is understood that the R term is evaluated as described in Appendix II.

In calculating the mutual impedance between the ith and jth currents within a package, it is convenient to split the computation into two parts

$$\begin{aligned}Z_{ij}^{xx} &= -\int\int dx\, dy\, f_i(x)\, g_i(y)[E_x^{\text{pri}} + E_x^{\text{img}}]_j \qquad (15a) \\ &= Z_{ij}^{\text{pri}} + Z_{ij}^{\text{img}} \qquad (15b)\end{aligned}$$

where

$$\begin{aligned}Z_{ij}^{\text{pri}} &= -\int\int dx\, dy\, f_i(x)\, g_i(y) \\ &\quad \cdot \int\int dx'\, dy'\, f_j(x')\, g_j(y') G_{xx} \qquad (15c)\end{aligned}$$

$$\begin{aligned}Z_{ij}^{\text{img}} &\approx -\langle J_{xi}\rangle \langle J_{xj}\rangle \left(\frac{-j}{2\beta_o^{\text{TM}}}\right) \\ &\quad \cdot \text{Res}[Q_{\text{TM}}(\beta_o^{\text{TM}})] \frac{\partial^2}{\partial x_i^2} \sum_{\alpha,\beta} \\ &\quad \cdot s_\beta H_o^{(2)}(\beta_o^{\text{TM}} \sqrt{(x_i - x_\alpha)^2 + (y_i - y_\beta)^2}) \qquad (15d)\end{aligned}$$

and again it should be noted that a more explicit, computationally efficient expression for the double summation in (15d) is described in Appendix II. The mutual impedance between the primary currents, Z_{ij}^{pri}, is calculated by inserting (2a) and (3) into (15c) exactly as if the currents were located in a laterally open structure. When the currents are located close to one another a spectral integration is necessary. Z_{ij}^{pri} is slowly varying with respect to frequency and thus its value over a broad range of frequencies can be evaluated by computing only a few points in a band and then interpolating to evaluate it at all other frequencies. In addition, Z_{ij}^{pri} depends only on the relative location of i, j and this leads to a number of useful redundancies when a uniform grid is used. The image contribution, Z_{ij}^{img} does not depend upon the details of the ith or jth current element, only on their average values. It can be calculated very quickly, but is very frequency dependent especially if the enclosure is large, has many resonances, and is high Q. It should be noted that for a lossless enclosure, the real part of the self terms in (15a) is zero. Thus a check case is that real self impedance in (15c) is the negative of the real self impedance in (15d) for a lossless enclosure.

IV. Package Effect Results

In order to investigate enclosure effects and the accuracy of the TM_o approximation, a microstrip dipole MMIC circuit is analyzed. This dipole exists on the surface of a GaAs substrate and has a full wavelength resonance near 56 GHz. Referring to Fig. 1 the layer structure is $d_1 = 0.1\,\text{mm}, d_2 = 0.3\,\text{mm}, d_3 = 0.1\,\text{mm}, \epsilon_{r1} = 12.7, \epsilon_{r2} = 1.0$, and $\epsilon_{r3} = 12(1-j)$. The dipole is 1.55 mm long and 0.2 mm wide. It is excited by an ideal gap generator located at the dipole's center. The moment method is applied by expanding the dipole current in terms of eleven x directed rooftop basis functions.

Fig. 4 shows a plot of the real part of the impedance seen by the gap generator versus frequency. When no side walls are present only one peak, at the dipole resonance, is evident. It turns out that the non-infinite Q of the dipole resonance is primarily due to radiation of TM_o parallel plate wave energy and not the presence of the lossy cover substrate (making the cover layer lossless has little effect). For the no side wall analysis, only the moment method impedance matrix elements of Z^{pri} (as defined in (15c)) are necessary and these are calculated using the conventional full spectral integration in (3) (see also [9]). The impedances were calculated at only three frequencies and interpolation was used to determine their values at the other 80 frequencies in the band.

If the dipole is centered at $x, y = 0$ and lateral side walls are introduced at $W_1 = 3.77\,\text{mm}, W_2 = -2.70\,\text{mm}, W_3 = -6.23\,\text{mm}$ and $W_4 = 3.30\,\text{mm}, Z^{\text{img}}$ is no longer zero. It must be calculated at each of the 80 frequencies shown in the

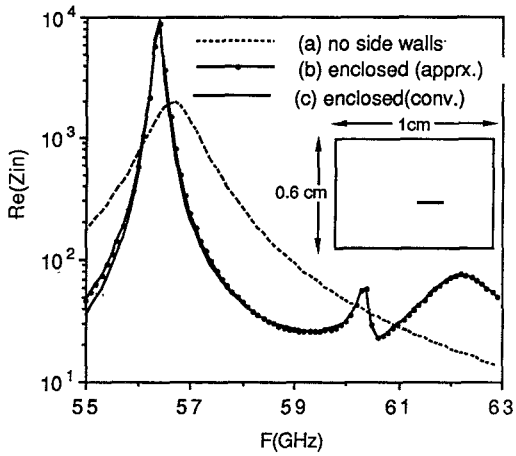

Fig. 4. Frequency response of the real part of the input impedance (in ohms) of a dipole in a layered medium with (a) no sidewalls. (b) lateral enclosure effects calculated using the TM_0 approximation, and (c) lateral enclosure effects calculated using the full spectrum.

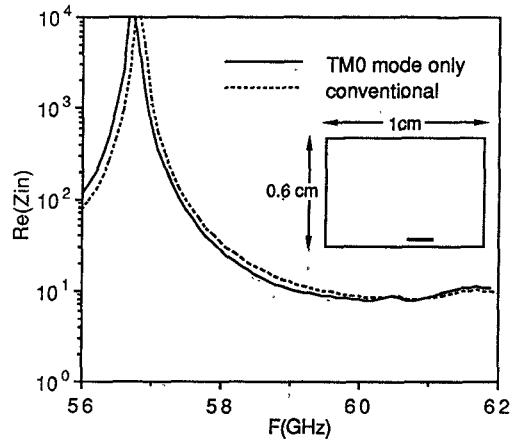

Fig. 5. Dipole resistance for a dipole 0.5 mm from side wall. A conventional calculation is compared to the TM_0 approximation.

figure—a quick calculation. Adding Z^{img} to Z^{pri} and solving for the current leads to the impedance seen by the gap generator with the dipole fully enclosed. Fig. 4 shows this result. Note that the apparent Q of the dipole resonance increases when side walls are added and that package resonances at 60, 61, and 61.7 GHz are introduced. If a lossy cover substrate were not present in the enclosure, all of these resonances would generate infinities in this plot. Fig. 4 also shows the enclosed dipole impedance computed using completely different software based on a conventional moment solution [14] where a long spectral summation is usually necessary at each frequency. The curves are almost identical, thus showing the accuracy of the TM_o approximation.

In Fig. 5 both the approximate and conventional solutions are plotted when the dipole edge is within 0.5 mm of wall 2 ($W_1 = 3.78\,\text{mm}, W_2 = -0.6\,\text{mm}, W_3 = -6.23\,\text{mm}$ and $W_4 = 5.4\,\text{mm}$). The two curves are in good agreement even though the near image in wall 2 is only 1 mm away. If the dipole is moved to within 0.2 mm of wall 1 ($W_1 = 0.975\,\text{mm}, W_2 = -2.700\,\text{mm}, W_3 = -9.025\,\text{mm}$ and $W_4 = 3.300\,\text{mm}$), the agreement is similarly good. Again this shows that the TM_o mode alone is the most important coupling mechanism for this cover height.

Table I shows the effect that increasing the cover height can have. All the parameters are the same as in Fig. 5 except that d_2 is increased by various amounts. For each of three different values of d_2, Z^{img} is calculated using increasing numbers of parallel plate modes. Z^{img} and Z^{pri} are then combined and used to calculate the input resistance seen by the gap generator. This resistance is tabulated. For a cover height of 1 mm ($d2 = 0.8$), only the TM_0 mode is necessary and additional modes have very little effect. As the cover height increases the TE_1 mode becomes less cut off and as a result the dipole feels the effect of the dipole image reactive fields. For a cover height of 1.8 mm, the TE_1 is close to turning on and has an important effect on the calculation. Thus one can always check the accuracy of the TM_0 approximations by adding TE_1, TM_1, ... corrections to the mutual impedance

TABLE I
CONVERGENCE OF THE REAL PART OF Z_{in} AT 60 GHz FOR INCREASING COVER HEIGHTS AND INCREASING NUMBER OF IMAGE COUPLING MODES. ENCLOSURE PARAMETERS ARE: $d_1 = 0.1\,\text{mm}, d_3 = 0.1\,\text{mm}, \epsilon_{r_1} = 12.7, \epsilon_{r_2} = 1.0, \epsilon_{r_3} = 12(1-j)$, $W_1 = 3.77\,\text{mm}, W_2 = -0.6\,\text{mm}, W_3 = -6.23\,\text{mm}$ and $W_4 = 5.4\,\text{mm}$

modes \ d2	0.8mm	1.3mm	1.8mm
TM_0	44.89	1.122	0.4204
TM_0,TE_1	44.97	2.831	10.16
TM_0,TE_1, TM_1	44.97	2.842	9.892
TM_0,TE_1, TM_1,TE_2	44.97	2.848	9.942

expressions and looking for any change in the result. This is easy to do codewise and is an important quality of this approach. Note again that the dipole is very close to the side wall. In most cases the circuit under consideration is not so near a wall and only the TM_0 correction is necessary.

Finally, consider the dipole located in a large package with dimensions 1.2 cm by 2.0 cm ($W_1 = 6.78\,\text{mm}, W_2 = -5.5\,\text{mm}, W_3 = -13.2\,\text{mm}$ and $W_4 = 6.5\,\text{mm}$) and with all other parameters the same as those used for the results in the previous calculations except that $d2 = 0.5\,\text{mm}$. Fig. 6 shows the real part of the dipole impedance as the Q of the package is reduced by increasing the loss tangent of the cover substrate. For comparison, the laterally unenclosed dipole resistance is also plotted. When the loss tangent of the cover substrate is 1 and 10, the Q of the cavity is about 60 and 15 respectively for the 8 resonances that occur in this bandwidth. The figure shows that the response of the dipole approaches the unenclosed response for the lower Q case, but still differs. Since this difference depends upon the dipole's location in the package, it is undesirable (The curve labeled "open" in Fig. 6 does not change substantially as the cover substrate loss tangent is varied.). It turns out that a further increase in the cover substrate loss tangent does not result in a further reduction in enclosure Q. In fact, the Q starts to increase since the cover layer starts to look like a conductor. Thus for a package of this size with these substrate dimensions and permittivities,

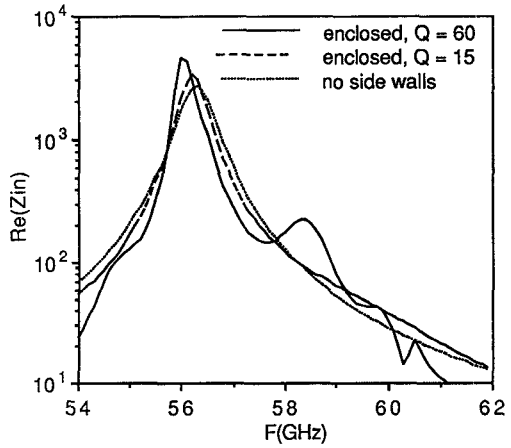

Fig. 6. Dipole resistance in a large enclosure. Lowering enclosure Q causes the response to approach the response in the laterally open case.

the package resonances always affect the circuit behavior. Doubling the enclosure dimensions however will result in a curve which is identical to the unenclosed dipole curve for the loss tangent of 10. Also, decreasing d_2 will reduce Q and improve agreement. The point here is that it is not always completely obvious what to do in order to reduce resonance effects or whether they have been eliminated sufficiently for a particular application. Further discussion can be found in reference [16].

V. Circuits or Sources Located On or Near a Sidewall

The concept described in the previous section separates the circuit from its enclosure in as far as calculating the moment method matrix is concerned. It works very well for covered circuits located in the interior of the package, not too near a side wall. This is the situation for most of the circuitry on a large integrated circuit. However, if a gap generator on a side wall is to be used to excite a circuit, a modification in procedure must be made before the enclosure and the circuit can be separated. This is due to the fact that the generator excites feed line currents that are on or near one side wall. Thus the nearest image in the side wall is close enough that all the image reactive fields contribute to the field evaluated at a near interior point. The higher order images in the near side wall and all the images in the other three side walls are still far enough away so that only the TM_0 wave communicates their contribution. Calculating the mutual impedance between two laterally enclosed near wall currents is again viewed as testing the field due to a primary current source and all of its image sources. Again, these sources are divided into two groups, but the division is different than in the previous section.

The first group consists of the primary current and its near image. Their contribution to the field at the testing point is calculated first. The full spectrum involving (1), (2) and (3) is used in this calculation. Fig. 7 shows this schematically. For example, expansion current 4 and its image, $4'$, are equal amplitude and co-directed. They generate a field that is tested by, say, function 2. A special case occurs for the expansion half current adjacent to the wall. It and its image form one current which straddles the wall. Also, if the gap generator

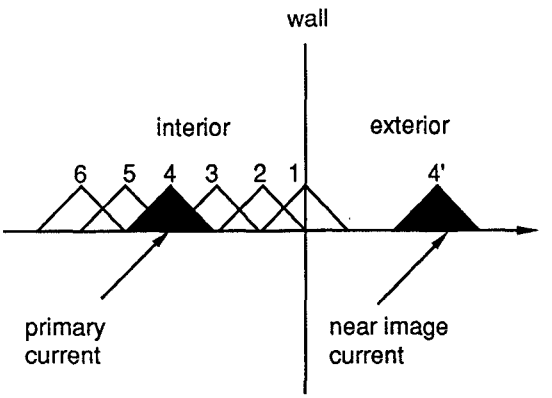

Fig. 7. Schematic of expansion currents and a representative image current near, and on, a sidewall.

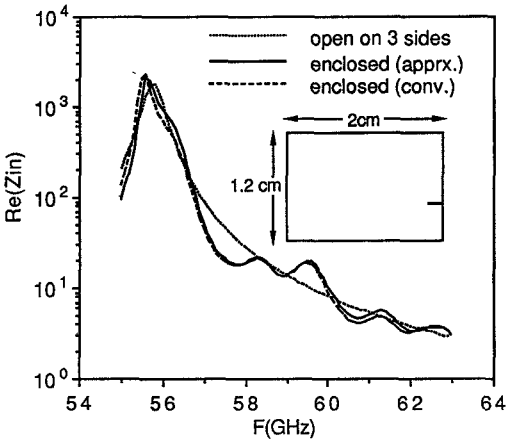

Fig. 8. Input resistance of an open circuit stub protruding from a side wall.

adjacent to the wall is of strength V, testing the total field from currents 1–6 and $2'$–$6'$ with current 1 gives $2V$ volts due to the fact that both the gap generator and its image contribute. A method of moments matrix equation can be calculated in this manner. The resulting solution is for a gap generator on a wall driving a stub in a laterally unbounded half space. One of the curves in Fig. 8 shows the real part of the impedance seen by the gap source exciting a microstrip stub of width 0.2 mm protruding 0.775 mm from the right-hand wall. Since the stub is not enclosed on three sides, there are no enclosure resonances in that one curve. Six rooftop expansion currents were used including the one straddling the wall.

The second group of currents consists of the images that are introduced when the three remaining walls are included in the problem. These image sources are far from the interior field points and their contribution to the tested fields can be computed using the TM_0 assumption implicit in (14). The near wall image contribution has already been counted as described previously and thus must be excluded from this calculation. One way of organizing this calculation is as follows. Assuming the source is located on the $x = W_1$ wall, one calculates the effect of the far images by placing the primary current and its near image in a new package with dimensions 2a by b. The currents straddle the center line of the new package at $x = W_1$ as shown in Fig. 9. The package contributions (minus

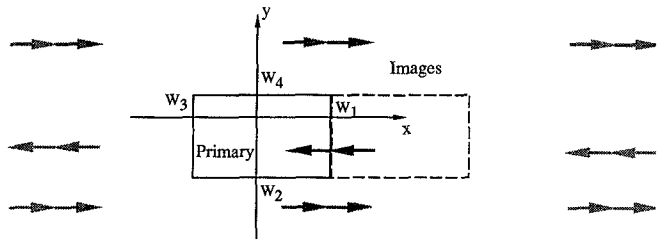

Fig. 9. Schematic showing how the image currents, excluding the near image current, can be treated as though the primary current and its near image are in a 2a × b enclosure.

near image) to the mutual impedance between the ith testing function and the jth expansion function is

$$Z_{ij}^{\text{img}} \approx -\langle J_{xi}\rangle\langle J_{xj}\rangle\left(\frac{-j}{2\beta_o^{\text{TM}}}\right)\text{Res}[Q_{\text{TM}}(\beta_o^{\text{TM}})] \cdot \frac{\partial^2}{\partial x^2}\left[\sum_{\alpha,\beta} s_\beta H_o^{(2)}(\beta_o^{\text{TM}}\sqrt{(x_i-x_\alpha)^2+(y_i-y_\beta)^2} + \sum_{\alpha',\beta'} s_{\beta'} H_o^{(2)}(\beta_o^{\text{TM}}\sqrt{(x_i-x_{\alpha'})^2+(y_i-y_{\beta'})^2})\right] \tag{17}$$

where the x_α, y_β coordinates locate the images of the primary current in the 2a × b box and the $x_{\alpha'}, y_{\beta'}$ coordinates locate the images of the near wall image current in the 2a × b box. Again the summations in (17) are calculated efficiently via the method described in Appendix II.

Combining the impedance calculations for both of the aforementioned groups results in the method of moments matrix for the circuit in an enclosure of dimensions a × b. Fig. 8 shows the real part of the input impedance when the stub described previously extends from the W_1 wall and the gap generator source centered at $x = 0, y = 0$ and $W_1 = 0, W_2 = -5.0\,\text{mm}, W_3 = -20.0\,\text{mm}, W_4 = 7.0\,\text{mm}$. The enclosure introduces several variations in the impedance which are not present without the enclosure. These are due to package resonances. The results using the conventional technique [14] are also shown for comparison. Excellent agreement is apparent.

VI. Conclusion

The formulation described in the preceding sections allows one to calculate a circuit's terminal characteristics with and without a lateral enclosure. It also improves numerical efficiency for calculations in large enclosures. The lateral enclosure correction is calculated by summing the fields contributed by the circuit's sidewall images. This can be accomplished very efficiently due to the fact that only the TM_0 parallel plate mode communicates the image fields when the top conducting cover is not too far from the MMIC surface and when the circuit is not too close to a side wall—the majority of cases. If larger cover heights or closer walls are used, the calculation can be made as accurate as desired by including corrections due to higher order evanescent parallel plate waves. The efficiency of the enclosure calculation at a particular frequency does not depend on enclosure Q or size. A very simple circuit was analyzed using this formulation and the results compared to results generated by software employing a conventional formulation. Examples of convergence were presented.

Most circuits are launched from a side wall. In such cases the formulation must be modified. The portion of the circuit near the launch sidewall is first analyzed as though only the near wall and top and bottom conducting planes are present. No enclosure resonances occur in this calculation. Next the effect of the other three walls is added to the impedance matrix using the image summation described in the text. This step adds the effect of resonances. Again a simple stub protruding from a side wall was analyzed and compared to a conventional analysis of the same structure. We note that the results in this case are highly idealized and a practical coaxial side wall feed has added effects not modeled herein [7] although they could be. We further note that deembeding algorithms for removing idealized feed effects are often rendered invalid due to enclosure resonances [23]. The formulation described in this paper could be used to remove this problem.

Although this formulation will also work for high Q enclosures, its application will probably be most important for low Q enclosures. After all, no packaged MMIC will operate properly if high Q resonances occur in a frequency range of interest. A practical high frequency enclosure will always include some type of damping layer to reduce the enclosure Q. Furthermore, as mentioned in the introduction, the usual design procedure is to analyze a circuit piece in an analysis enclosure, get its terminal characteristics, and use them in a conventional circuit analysis of an entire MMIC. In all cases the analysis enclosure will be different than the final operating enclosure. The only way to take this effect out of the problem is to make sure that both enclosures are very low Q. Ideally the enclosure Q should be reduced far enough that the side walls are invisible to the circuit, creating an "anechoic" enclosure. However it is difficult to know how low is low enough since the effect of a low Q resonance becomes more of a subtle undulation in a circuit's frequency response. Also, the size of the undulation varies with position in the package. Thus a formulation such as the one described here would allow the differences, with and without the enclosure, to be assessed.

Appendix I

The following notation describes Fourier transform Green's function for the layered structure in Fig. 1. Note that $V = E$ or M

$$Q_{\text{TV}} = \frac{1}{Y_{\text{LV}}^{(1)} + Y_{\text{RV}}^{(2)}} = \frac{1}{Y_V} \tag{A1a}$$

$$Y_{\text{LV}}^{(1)} = -jY_{\text{TV}}^{(1)}\cot(k_{z1}d_1)$$

$$Y_{\text{RV}}^{(3)} = -jY_{\text{TV}}^{(3)}\cot(k_{z3}d_3) \tag{A1b}$$

$$Y_{\text{RV}}^{(2)} = Y_{\text{TV}}^{(2)}\frac{Y_{\text{RV}}^{(3)} + jY_{\text{TV}}^{(2)}\tan(k_{z2}d_2)}{Y_{\text{TV}}^{(2)} + jY_{\text{RV}}^{(3)}\tan(k_{z2}d_2)} \tag{A1c}$$

$$Y_{\text{TM}}^{(i)} = \frac{\epsilon_{ri}k_o}{k_{zi}\eta_o} \qquad Y_{\text{TE}}^{(i)} = \frac{k_{zi}}{k_o\eta_o}$$

$$k_{zi}^2 = \epsilon_{ri}k_0^2 - \beta^2 \qquad \text{Im}(k_{zi}) < 0$$

APPENDIX II

In what follows, the double summation in (13b) is written in terms of a single summation which converges very quickly. Define ΣH by,

$$\Sigma H = \sum_{\alpha}\sum_{\beta} s_\beta \cdot H_0^{(2)}(\beta_o^{\mathrm{TM}}\sqrt{(x-x_\alpha)^2+(y-y_\beta)^2}) \quad \text{(A2)}$$

where the current locations (x_α, y_β) have not yet been explicitly defined.

First note that the image currents described by (12) can be split into three groups

$$J_{xj}^{+} = g_j^t(y)\sum_{n=1}^{\infty}[f_j(x-2an)+f_j(2W_3-x+2an)] \quad \text{(A3a)}$$

$$J_{xj}^{-} = g_j^t(y)\sum_{n=-\infty}^{-1}[f_j(x-2an)+f_j(2W_1-x+2an)] \quad \text{(A3b)}$$

$$J_{xj}^{o} = f_j(x)\sum_{m=1}^{\infty}[g_j(y\pm 2bm) - g_j(2W_2-y+2bm) - g_j(2W_4-y-2bm)] \quad \text{(A3c)}$$

where f_j and g_j are non-zero in a small region centered around x_j and y_j. The first and second groups of image currents are located in regions $x > W_1$ and $x < W_3$ respectively. The third includes all the remaining image currents. These form a linear array of currents extending above and below the package in the range $W_3 < x < W_1$ (refer to Fig. 3).

First consider the contribution of the first group to ΣH. From the definition of $g_j^t(y)$ in equation (11c) we know that the currents in (A3a) are located at the y coordinates, $y_\beta = y_j + 2mb$ and $y_\beta = 2W_4 - y_j + 2mb$ with the latter currents having negative signs ($s_\beta = -1$). Thus the contributions to ΣH from these currents are

$$\Sigma H^{+} = \sum_{\alpha}\sum_{m=-\infty}^{\infty} \cdot [H_0^{(2)}(\beta\sqrt{(x-x_\alpha)^2+(y-y_j-2mb)^2}) - H_0^{(2)}(\beta\sqrt{(x-x_\alpha)^2+(y-2W_4+y_j-2mb)^2})] \quad \text{(A4)}$$

where x_α is not explicitly defined for now.

Use the identity

$$H_0^{(2)}(\beta|\vec{\rho}-\vec{\rho}'|) = \int_{-\infty}^{\infty}\frac{dk_y}{\pi}\frac{e^{-jk_x|x-x'|}}{k_x}\cdot e^{jk_y(y-y')} \quad \text{(A5)}$$

where $k_x^2 = \beta^2 - k_y^2$ and $\mathrm{Im}(k_x) < 0$. And then use Poisson's formula,

$$\sum_{m=-\infty}^{\infty} e^{jk_y 2mb} = \sum_{m=-\infty}^{\infty}\frac{\pi}{b}\delta\left(k_y - \frac{m\pi}{b}\right) \quad \text{(A6)}$$

to simplify (A4) to

$$\Sigma H^{+} = \sum_{\alpha}\sum_{m=-\infty}^{\infty}\frac{1}{k_x}e^{-jk_x|x-x_\alpha|}T(m,y,y_j) \quad \text{(A7)}$$

where

$$T(m,y,y_j) = \frac{4}{b}\sin\left[\frac{m\pi}{b}(W_4-y)\right].\sin\left[\frac{m\pi}{b}(W_4-y_j)\right]. \quad \text{(A8)}$$

From (A3a) we see that the x coordinate that locates the image currents in the $x > W_1$ region can be explicitly determined to be $x_\alpha = x_j + 2na$ and $x_\alpha = 2W_3 - x_j + 2na$ with $n = 1,2,3\cdots\infty$. Expression (A7) now becomes,

$$\Sigma H^{+} = \sum_{m=1}^{\infty}\frac{T(m,y,y_j)}{k_x}\sum_{n=1}^{\infty}e^{-jk_x 2an} \cdot [e^{jk_x(x-x_j)} + e^{jk_x(x-2W_3+x_j)}] \quad \text{(A9)}$$

The same procedure can be applied to the image currents defined by (A3b) located in the $x < W_3$ region. The x_α coordinates which locate these image currents are $x_\alpha = x_j - 2na$ and $x_\alpha = 2W_1 - x_j - 2na$ with $n = 1,2,3\cdots\infty$. The contribution of these currents to (A2) is

$$\Sigma H^{-} = \sum_{m=1}^{\infty}\frac{T(m,y,y_j)}{k_x}\sum_{n=1}^{\infty}e^{-jk_x 2an} \cdot [e^{-jk_x(x-x_j)} + e^{-jk_x(x-2W_1+x_j)}] \quad \text{(A10)}$$

Adding equation (A9) and (A10) and reducing the n index summation to closed form results in the expression,

$$\Sigma H^{+} + \Sigma H^{-} = \sum_{m=1}^{\infty}\frac{T(m,y,y_j)e^{-jk_x a}U(k_x,x,x_j)}{k_x\sin(k_x a)} \quad \text{(A11a)}$$

where $k_x^2 = \beta^2 - (m\pi/b)^2$ $\mathrm{Im}(k_x) < 0$, and

$$U(k_x,x,x_j) = \left[e^{jk_x(x-x_j)} + e^{jk_x(x-2W_3+x_j)} + e^{-jk_x(x-x_j)} + e^{-jk_x(x-2W_1+x_j)}\right] \quad \text{(A11b)}$$

The only remaining image sources not included in (A11) are located above and below the package at $x_\alpha = x_j$ and $y_\beta = y_j \pm 2mb$ for $s_\beta = 1$ and also at $x_\alpha = x_j$ and $y_\beta = y_j + 2mb, y_\beta = 2W_2 - y_j + 2mb$ for $s_\beta = -1$. As before $m = 1,2,3\cdots$. Their contribution to ΣH is

$$\Sigma H^{o} = \sum_{m=1}^{\infty} V(m,x,x_j,y,y_j) \quad \text{(A12a)}$$

where

$$V(m,x,x_j,y,y_j) = H_0^{(2)}(\beta[(x-x_j)^2+(y-y_j\pm 2mb)^2]^{1/2}) - H_0^{(2)}(\beta[(x-x_j)^2+(y-2W_2+y_j-2mb)^2]^{1/2}) - H_0^{(2)}(\beta[(x-x_j)^2+(y-2W_4+y_j+2mb)^2]^{1/2}) \quad \text{(A12b)}$$

In practice V can be evaluated using the large argument approximation for $H_0^{(2)}$.

In summary then, combine (A11) and (A12) to get the full expression for ΣH,

$$\Sigma H = \sum_{m=1}^{\infty} \left\{ \frac{T(m, y, y_j) e^{-jk_x a} U(k_x, x, x_j)}{k_x \sin(k_x a)} + V(m, x, x_j, y, y_j) \right\} \quad \text{(A13)}$$

Substituting this expression for the double summation in (13b) and then in (14) gives the field at x, y within the package due to only the images of a current element located at x_j, y_j. The summation in (A13) can be truncated after only a few terms ($\sim$10) and thus it can be quickly evaluated.

A package resonance occurs when $\mathrm{Re}[k_x a] = 0, \pi, 2\pi \cdots$ due to the sine factor in the denominator of (A13). The Q at resonance is determined by the size of the imaginary part of k_x which is in turn dependent on the size of the imaginary part of β. In most cases $\beta = \beta_0^{\mathrm{TM}}$ and thus the imaginary part of the propagating parallel plate mode determines the Q. However, the expression (A13) can also be used if β is primarily imaginary, as it is if $\beta = \beta_1^{\mathrm{TM}}$ or $\beta = \beta_1^{\mathrm{TE}}$ are used to check the accuracy of the TM_o approximation.

REFERENCES

[1] R. H. Jansen, "Hybrid mode analysis of end effects of planar microwave and millimeter wave transmission lines," *Proc. Inst. Elec. Eng.*, vol. 2128, pt. H., pp. 77–86, Apr. 1978.

[2] J. Boukamp and R. H. Jansen, "The high frequency behavior of microstrip open ends in microwave integrated circuits including energy leakage," in *Proc. 14th European Microwave Conf.*, 1984, pp. 142–147.

[3] R. W. Jackson and D. M. Pozar, "Microstrip open-end and gap discontinuities," *IEEE Trans. Microwave Theory Tech.*, vol. MTT-33, pp. 1036–1042, Oct. 1985.

[4] R. H. Jansen, "The spectral domain approach for microwave integrated circuits," *IEEE Trans. Microwave Theory Tech.*, vol. MTT-33, pp. 1043–1056, 1985.

[5] P. B. Katehi and N. C. Alexopoulos, "Frequency-dependent characteristics of microstrip discontinuities in millimeter-wave integrated circuits," *IEEE Trans. Microwave Theory Tech.*, vol. MTT-33, pp. 1029–1035, Oct. 1985.

[6] Y. L. Chow *et al.*, "A modified moment method for the computation of complex MMIC circuits," in *Proc. 16th European Microwave Conf.*, 1986, pp. 625–630.

[7] J. C. Rautio and R. F. Harrington, "An electromagnetic time-harmonic analysis of shielded microstrip circuits," *IEEE Trans. Microwave Theory Tech.*, vol. MTT-35, pp. 726–730, Aug. 1987.

[8] J. R. Mosig, "Arbitrarily shaped microstrip structures and their analysis with a mixed potential integral equation," *IEEE Trans. Microwave Theory and Tech.*, vol. 36, pp. 314–323, February 1988.

[9] R. W. Jackson, "Full-wave finite element analysis of irregular microstrip discontinuities," *IEEE Trans. Microwave Theory Tech.*, vol. 37, pp. 81–89, January 1989.

[10] R. H. Jansen, "Modular source-type 3D analysis of scattering parameters for general discontinuities, components and coupling effects in (M)MIC's," in *17th European Microwave Conf. Proc.*, Rome, Italy, 1987, pp. 427–432.

[11] L. P. Dunleavy and P. B. Katehi, "A generalized method for analyzing shielded thin microstrip discontinuities," *IEEE Trans. Microwave Theory Tech.*, vol. 36, pp. 1758–1766, Dec. 1988.

[12] W. Wertgen and R. H. Jansen, "Efficient direct and iterative electrodynamic analysis of geometrically complex MIC and MMIC structures," *Int. J. of Numerical Modeling*, vol. 2, pp. 153–186, 1989.

[13] A. Hill and V. K. Tripathi, "An efficient algorithm for the three-dimensional analysis of passive microstrip components and discontinuities for microwave and millimeter-wave integrated circuits," *IEEE Trans. Microwave Theory Tech.*, vol. 39, pp. 83–91, Jan. 1991.

[14] J. J. Burke and R. W. Jackson, "Reduction of parisitic coupling in packaged MMIC's," in *IEEE MTT-S Int. Microwave Symp. Dig.*, May 1990, pp. 255–258.

[15] R. W. Jackson, "Frequency domain modeling of MMICs including package effects, presented at the "Workshop on New Developments in Numerical Modeling of Microwave and Millimeter Wave Structures," *IEEE MTT-S Int. Microwave Symp. Dig.*, Dallas, May 1990.

[16] ——, "Removing package effects from microstrip moment method calculations," *IEEE MTT-S Int. Microwave Symp. Dig.*, vol. June 1992, pp. 1225–1228.

[17] R. H. Jansen and L. Wiemer, "Full-wave theory based development of MM-wave circuit models for microstrip open end, gap, step, bend and tee," *IEEE MTT-S Int. Microwave Symp. Dig.*, June 1989, pp. 779–782.

[18] R. J. Arnold, R. H. Jansen and L. Weimer, "Microstrip discontinuity models to 60 GHz," Final Technical Report RL-TR-91-198, Rome Laboratory, Air Force Systems Command Griffiss AFB, New York, Aug. 1991.

[19] J. J. Burke and R. W. Jackson, "A simple circuit model for resonant mode coupling in packaged MMICs," in *IEEE MTT-S Int. Microwave Symp. Dig.*, Boston, June 1990.

[20] R. H. Jansen and J. Sauer, "High-speed 3D electromagnetic simulation for MIC/MMIC CAD using the spectral operator expansion (SOE) technique," *IEEE MTT-S Int. Microwave Symp. Dig.*, June 1991, pp. 1087–1090.

[21] T. Itoh, "Spectral domain immitance approach for dispersion characteristics of generalized printed transmission lines," *IEEE Trans. Microwave Theory Tech.*, vol. MTT-28, pp. 33–736, July 1980.

[22] Y. L. Chow, J. J. Yang, and D. G. Fang, "Closed form Green's function of open or shielded microstrip structure," in *1990 IEEE Antennas and Propagation Symp. Dig.*, Dallas, Vol II, May 1990, pp. 622–626.

[23] J. C. Rautio, "A De-Embedding Algorithm For Electromagnetics," *Int. J. of Microwave & Millimeter-Wave Computer - Aided Engineering*, vol. 1, no. 3, July 1991.

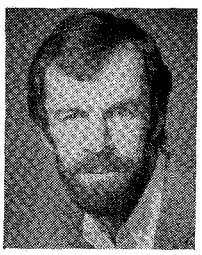

Robert W. Jackson (M'82–SM'88) was born in Boston, MA in 1952. He received the B.S. (1975), M.S. (1979), and Ph.D. (1981) degrees in electrical engineering from Northeastern University, Boston. His dissertation was concerned with nonlinear plasma interactions in the low shock of the earth.

From 1981 to 1982, he was an Assistant Professor in the Department of Electrical Engineering at Northeastern University. Since 1982, he has been on the faculty of the Department of Electrical and Computer Engineering at the University of Massachusetts at Amherst, where he is currently an Associate Professor. His research interests include the electromagnetic aspects of integrated circuits, novel printed circuit and antenna structures, modeling and design of planar ferrite devices, electromagnetics applied to nonlinear or anisotropic materials, and active microwave circuit design.